Volume 1 | Number 1 | Jan 2013 | Pages 1–100

Journal of
Materials Chemistry B

Materials for biology and medicine
www.rsc.org/materialsB

ROYAL SOCIETY
OF CHEMISTRY

ROYAL SOCIETY
OF CHEMISTRY

www.rsc.org/materialsB

Journal of Materials Chemistry B

RSCPublishing

ARTICLE

In vitro antibacterial capacity and cytocompatibility of SiO2–CaO–P2O5 meso-macroporous glass scaffolds enriched with ZnO

Sandra Sánchez-Salcedo[a,b,c], Shruti Shruti[a,d], Antonio J. Salinas[a,b,c]*, Gianluca Malavasi[d], Ledi Menabue[d], Maria Vallet-Regí[a,b,c]*

Zn^{2+} ions exhibit osteogenic, angiogenic and antimicrobial properties. For this reason, they are often added in small amounts to bioceramics investigated for bone tissue engineering. In this paper, the cytocompatibility and antibacterial properties of $80\%SiO_2$–$15\%CaO$–$5\%P_2O_5$ (mol%) mesoporous bioactive glass (MBG) scaffolds substituted with 4.0% and 7.0% of ZnO were studied and compared with the Zn-free scaffold. Cell proliferation, morphology, differentiation and cytotoxic effects of Zn^{2+} ions released from samples were examined by culturing HOS osteoblasts both in the presence of sample extracts and on the scaffolds surface. The bacterial inhibition capacity of the scaffolds was explored by using gram-positive *S. aureus* bacteria, responsible for numerous infections in orthopedic surgery, and simulating a severe infection. Our results show that Zn-MBG scaffolds possess hierarchical meso-macropore structure suitable for osteoblast growth. Furthermore, the amount of Zn^{2+} ions released from the scaffold with 4.0% ZnO was found to be more favorable for HOS cell development than that released from the scaffold including 7.0% ZnO. Besides, Zn^{2+} released to medium from both scaffolds exhibited antibacterial properties against *S. aureus* bacteria. Hence, cytocompatibility and antibacterial ability showed by MBG scaffold containing 4.0% ZnO makes it a suitable candidate for bone regeneration applications.

1. Introduction

Post-operative bacterial infection is one of the major issues associated with the treatment of bone fractures and diseases with implants. This problem affects 2% of joint prostheses and 5% of fracture fixation devices implanted.[1,2] Mostly prosthetic joint infections are produced by *Staphylococcus Aureus* and *Staphylococcus Epidermidis*[3,4] that has a considerable financial consequence for both patient and healthcare provider.[5–7] Bacteria form a biofilm hindering antibiotics to reach the infected area. Thus, making it necessary a surgical intervention which further increases the effective cost.[8]

SiO2–CaO–P2O5 mesoporous bioactive glasses (MBGs) exhibiting ordered arrangement of mesopores (pore diameter: 2–10 nm),[9,10] are widely investigated to synthesize scaffolds used in bone regeneration applications.[11,12] These materials exhibit the quickest in vitro bioactive response reported for a synthetic material.[13] Furthermore, they display high surface area and pore volume suitable to host biologically significant molecules.[14–16] For these reasons, the processing of MBGs into 3D scaffolds with interconnected macropores (100–1000 μm), required for tissue ingrowths and vascularization,[17,18] is a subject of great interest. In this context, rapid prototyping processing[19] has revealed as a successful method to obtain macro-mesoporous bioactive scaffolds in the SiO2–CaO–P2O5 system.[20,21]

The ideal scaffolds used in bone tissue engineering must promote bone formation by stimulating osteogenesis and angiogenesis along with more features like anti-inflammatory or antimicrobial effects.[22–24] One of the strategies to upgrade the biological behaviour of MBG scaffolds is by adding to the glass small amounts of so called therapeutic inorganic ions such as Zn^{2+}, Cu^{2+}, Mg^{2+}, Co^{2+}, Ga^{3+} or Ce^{3+}.[25–27] Synthesis parameters, in vitro bioactivity and controlled drug release ability of Zn-substituted MBGs were already investigated.[28–30] Furthermore, the structure and bioactivity of MBGs compared with analogous glasses, obtained by sol–gel, has been reported.[31] Zn exerts an important effect in bone development, formation and metabolism,[32,33] as well as in the blood vessels growth.[34] It was reported that the slow release of Zn^{2+} ions from an implant promotes bone formation.[35] Moreover, its release inhibits the bacterial growth at the surgical site and improves wound healing.[36,37] For these reasons, Zn-containing glasses are investigated for orthopedic

applications.[18,38] Although it is necessary that it does not reach cytotoxic levels in plasma.[39,40]

This article focuses in the evaluation of the biocompatibility and antimicrobial properties of adding up to 7.0 mol% of ZnO to 80%SiO$_2$–15%CaO–5%P$_2$O$_5$ meso–macroporous scaffolds obtained by rapid prototyping. Biocompatibility will be investigated in terms of cell proliferation, morphology, differentiation and cytotoxic effect of scaffolds on osteoblast-like cells in both extracts and directly on the scaffolds surface. The antibacterial capabilities of the scaffolds will be evaluated using *S. Aureus* as model bacteria under physiological conditions, simulating a severe infection. In all the cases, the results of Zn-containing scaffolds will be compared with the Zn-free glass that will be denoted as "B".

2. Materials and Methods

2.1. Fabrication of MBG scaffolds by rapid prototyping: 3D printing

Mesoporous bioactive glasses of composition (80-x)%SiO$_2$–15%CaO–5%P$_2$O$_5$–x% additional oxide, being x= 0, 4% ZnO or 7% ZnO, (in mol%) were synthesized according to a method previously described.[28] Table S1 (Supporting Information) collects the composition of the synthesized mesoporous glass powders along with the amount of reactants used in their syntheses. Mesoporous glasses were obtained by evaporation induced self assembly process (EISA) using Pluronic® P123 (Sigma Aldrich) as surfactant. Tetraethyl orthosilicate (TEOS), calcium nitrate tetrahydrate, triethyl phosphate (TEP), and zinc nitrate hexahydrate (Sigma Aldrich) were used as sources of SiO$_2$, CaO, P$_2$O$_5$ and ZnO, respectively. These reactants were added to 85 mL of ethanol containing 4.5 g of dissolved P123 and 1.12 mL of 0.5 N HNO$_3$. The resultant sol was cast in a Petri dish followed by gelation, aging and drying at room temperature for 7 days. The dried gel was heated at 700°C for 3 h to remove the surfactant and then subjected to milling and sieving to obtain grains (under 32 μm) for the scaffolds preparation.

MBG scaffolds were obtained by rapid prototyping technique using EnvisionTEC GmbH 3D Bioplotter™ printing device. The technique involves reproducing a previous computer-aided design format by injecting a paste using a robot injector. The paste was obtained by suspending 4 g of MBG powder in 37 mL dicholoromethane (DCM) followed by addition of 2.6 g polycaprolactone (PCL) dissolved in the same quantity of DCM. This mixture was stirred at room temperature until it formed a paste with right consistency for injection. The paste was placed in a polyethylene cartridge fixed with a dispensing tip of 0.41 mm diameter and the rods spacing was set to 1.3 mm. Each layer was rotated to an angle of 45º to the next one, building rhombohedral channels. The speed of the tip was set at 300 mm min^{-1} in the horizontal plane and 50 mm min^{-1} in the vertical plane. The dimension of scaffolds was 8 mm x 8 mm x 3 mm and consisted of 8 layers. They were dried in an oven at 70ºC for 2 h to evaporate DCM and then treated at 500ºC for 3 h to remove PCL. Elemental analysis was performed in a Perkin Elmer 2400 CHN analyzer to determine any residual content of PCL.

2.2. Characterization of scaffolds

Powder X-ray diffraction experiments were performed with a Philips X'Pert diffractometer equipped with Cu Kα radiation (wavelength 1.5418 Å). XRD patterns were collected in the 2θ range between 0.6° and 8° with a step size of 0.02° and a counting time of 5 s per step.

The ordered structure of mesopopores was also evaluated by Transmission Electron Microscopy (TEM) in a JEOL JEM 2100 microscope, operating at 200 kV, equipped with an Energy Dispersive X-ray (EDX) (Oxford INCA) microanalysis stage.

Nitrogen adsorption – desorption isotherms at 77.35 K used to determine the textural properties were acquired in a Micromeritics ASAP 2020 porosimeter. Before the adsorption measurements, the samples were degassed under vacuum for 24 h at 120°C. The surface area was obtained by applying the Brunauer-Emmett-Teller (BET) method.[41] The pore size distribution was determined by the Barret-Joyner-Halenda (BJH) method from the adsorption branch of the isotherm.[42] Magic-angle-spinning (MAS) and single-pulse (SP) solid-state nuclear magnetic resonance (NMR) measurements were performed to evaluate the different silicon and phosphorus environments in the synthesized samples. The NMR spectra were recorded on a Bruker Model Avance 400 spectrometer. Samples were spun at 10 kHz for ^{29}Si and 6 kHz in the case of ^{31}P. Spectrometer frequencies were set to 79.49 and 161.97 MHz for ^{29}Si and ^{31}P, respectively. Chemical shift values were referenced to tetramethylsilane (TMS) and H$_3$PO$_4$ for ^{29}Si and ^{31}P, respectively. All spectra were obtained using a proton enhanced CP method, using a contact time of 1 ms. The time period between successive accumulations was 5 and 4 s for ^{29}Si and ^{31}P, respectively, and the number of scans was 10.000 for all the spectra.

The macroporosity of the scaffolds was examined by Scanning Electron Microscopy (SEM) in a JEOL 6400 microscope operating at 20 kV. Further, a preliminary test was performed to find out presences of pores on the surface and interconnection between the pores. Each scaffold was subjected to a red color dye dissolved in ethanol as previously reported.[30] Energy Dispersive X-ray (EDX) spectroscopy was also performed with the JEOL 6400 microscope to analyze the scaffolds composition. Each measurement was carried out in three specimens.

2.3. In vitro biocompatibility assays

In vitro biocompatibility assay was carried out using human osteoblast like cells (HOS cells, ECACC No. 87070202) denoted as HOS. The cell line is obtained through the European collection of cell cultures and was derived from osteoscarcoma of an old Caucasian female. Cells were cultured in Dulbecco's modified Eagle medium (DMEM) (Sigma Chemical Co., St. Louis, USA) at 37°C containing 2 mM glutamine, 100 U/mL penicillin, 100 μg/mL streptomycin and 10% Fetal Bovine Serum (FBS) (Life Technologies S.A., Spain) and working in a humidified atmosphere of 95% air and 5% CO$_2$. This medium hereinafter will be referred as complete medium. Osteoblast-like cells were routinely subcultured by trypsinization.

In vitro biocompatibility test was performed in two different ways: (i) A preliminary assay performed with scaffolds degradation products in order to understand the behavior of cells in the presence of released ions from scaffolds and to stabilize the conditions for biocompatibility assay. (ii) By culturing HOS cells directly on scaffolds surface. In both cases, HOS cells cultured in absence of degradation product and scaffolds were used as control. Prior to assays, B, 4.0Zn, 7.0Zn scaffolds were sterilized at 180 °C in an oven followed by UV-irradiation for 30 min. Then submerged in 2 mL of supplemented DMEM in 24-well tissue culture plates (Sarstedt,

Spain) under a 5% CO_2 atmosphere for 2 h at 37 ºC to remove possible initial burst of by-products of the synthesis process.[43]

2.3.1. In vitro biocompatibility of the degradation products of the scaffolds. B, 4.0Zn and 7.0Zn scaffolds were soaked in 2 mL complete medium under CO_2 (5%) atmosphere at 37°C for 2 and 4 days. At the end of each time interval, the complete medium (i.e. degradation products) was collected and filtered with 0.22 µm Millipore system filter. HOS cells were seeded into 24 well culture plate at a seeding density of 2.5 x 10^5 cell mL^{-1} in complete medium under CO_2 (5%) atmosphere at 37°C until they reached confluence. The complete medium was then replaced with degradation products collected after soaking scaffolds for 2 and 4 days. The cells were exposed to scaffolds degradation products for 24 h under CO_2 (5%) atmosphere at 37°C.

Mitochondrial activity of cells in contact with degradation products was measured by the MTT test. MTT assay is based on the activity of mitochondrial dehydrogenases of living cells that reduces yellow 3-[4.5-dimethylthiazol-2-yl]-2,5-diphenyltetrazolium bromide (MTT) to blue formazan and measured spectrophotometrically at 570 nm.[44] Cytotoxicity was evaluated in terms of lactate dehydrogenase (LDH) activity. LDH released from HOS cells is considered as measure of cell injury. The assay is based on reduction of NAD by LAD that converts tetrazolium dye forming a colored compound measured spectrophotometrically at 340 nm.[45] Measurements were made using Spinreact, a commercially available kit. Cell morphology was studied in the presence of the degradation products using Nikon eclipse TS100 inverted optical microscope equipped with a Nikon sight DS-U2 digital camera.

2.3.2. In vitro biocompatibility of the scaffolds. HOS cells were seeded on scaffolds in 24 well culture plate at a seeding density of 2.5 x 10^5 cell mL^{-1} in complete medium and incubated under CO_2 (5%) atmosphere at 37°C for different time periods.

The spreading degree and morphology of the osteoblast like cells were visualized by SEM in a JEOL JSM-6335F microscope after 2 days. The attached cells were rinsed twice with phosphate buffered saline (PBS) and fixed with 2.5% glutaraldehyde for 45 min in 0.1 M PBS. Sample dehydration was performed with slow water replacement by series of graded ethanol solutions (30%, 50%, 70%, 90%) with a final dehydration in absolute ethanol for 60 min. The materials were mounted on stubs, gold plated in vacuum using sputter coater (Blazer SCD 004 (Wiesbaden-Nordenstadt, Germany) and analyzed with SEM. Cell proliferation was determined in terms of cell mitochondrial activity by following the MTT (3-[4.5-dimethylthiazol-2-yl]-2,5-diphenyltetrazolium bromide) (Sigma-Aldrich, Spain) assay (described above) at 1, 3 and 6 days after seeding. The mitochondrial activity was measured both on the scaffold pieces and base of wells. Cell differentiation was evaluated by alkaline phosphatase (ALP) activity. Osteoblast-like phenotype was assessed by measuring ALP activity of HOS cells grown on different scaffolds. ALP activity was measured using the Reddi and Huggins method based on the hydrolysis of p-nitrophenylphosphate to p-nitrophenol.[46] For this HOS cells were seeded directly onto sample in 24 well plates and incubated in standard conditions using supplemented complete medium with β-glycerolposphate (50 µg, Life Technologies S.A., Spain) and L-ascorbic acid (Life Technologies S.A., Spain). ALP activity was determined after 7 and 21 days with the commercial available kit (Spinreact, Spain). The cell injury caused by the test samples was determined by released LDH from the cells. The

measurement was performed, as described above, using commercially available kit (Spinreact, Spain) at 1, 3 and 6 days after seeding.

2.3.3. Degradability of scaffolds in complete medium. To study the ionic release to medium, the scaffolds were soaked in 2 mL of DMEM supplemented with 10% FBS and antibiotics (100 U/mL penicillin, 100 mg/mL streptomycin) at 37 ºC between 3 h to 7 days. After each soaking times, the scaffolds were separated from 2 mL of DMEM solution. In each solution, calcium, silica, phosphorous, and zinc ions release from materials was determined by inductively coupled plasma/optical emission spectrometry (ICP/OES) using a Perkin Elmer OPTIMA 3300 DV device. In each analysis, the concentration of each ion was determined from 3 replicates on the same solution split in two independent experiments.

2.4. In vitro bacterial assay

The study was conducted to determine bactericidal activity of zinc substituted MBG scaffolds by using florescence test assay. Gram positive *Staphylococcus aureus* (ATCC 28213) was used as model bacteria. Prior to antibacterial growth assay, samples were sterilized by thermal treatment at 180°C for 2 h followed by soaking in 1 mL Todd Hewitt Broth (THB) medium (Sigma-Aldrich, USA) at 37°C for 2 h in order to stabilize samples for antibacterial assay.

2.4.1. Confocal Microscopy. Bacteria were grown in THB at 37°C under orbital stirring at 100 rpm until the optical density as measured at 600 nm reached 1 in a UV-VIS spectrometer (UV-530, Bonsai technologies, Spain). At this point the bacteria from culture (200 µL) were collected and resuspended in 3 mL THB which was incubated at 37°C until the optical density as measured at 600 nm reached 0.4. Then, the bacteria were diluted with THB to obtain 10^8 bacteria/ mL and different samples were soaked in 1 mL of this suspension for 48 h at 37°C. After 24 h, 500 µL of THB was replaced with fresh THB. After 48 h, the samples were stained with Invitrogen Live/Dead backlight bacterial viability kit,[47] washed with PBS and tested in a Biorad MC1025 confocal laser scanning microscope. SYTO 9 fluorescence was excited at 480/500 nm and the emitted fluorescence measured at 500 nm. Propidium iodide fluorescence was excited at 490/635 nm and the emitted fluorescence measured at 618 nm. Staining is performed with a mixture of dyes, SYTO 9 (live bacteria/green) and propidium iodide (dead bacteria/red) for 15 min in the dark and immediately observed. Each experiment has been carried out in three specimens split in two independent experiments. Three zones of each specimen of a surface of approximately 1.024 µm x 1.024 µm were captured in each image. The percentage of surface area covered with dead and live bacteria was calculated using ImageJ software (National Institute of Health Bethesda, MD, USA).

2.4.2 In vitro degradability of the scaffolds in THB

The evolution of ions released in THB medium was evaluated. The scaffolds were soaked in 2 mL of THB at 37 ºC between 3 hours to 7 days. After each soaking time, the scaffolds were separated from the 2 mL of THB solution. In each solution the calcium, silica, phosphorous, and zinc ions release from materials was determined by inductively coupled plasma/optical emission spectrometry (ICP/OES) using a Perkin Elmer OPTIMA 3300 DV device. In each analysis, the concentration of each ion was determined from 3 replicates on

tha same solution. Each experiment has been carried out in three specimens split in two independent experiments.

2.5. Statistics

Data obtained from biocompatibility and antibacterial assays are expressed as means ± standard deviations of the independent experiments indicated in each case. Statistical analysis was performed using the Statistical Package for the Social Sciences (SPSS) version 19 software. Statistical comparisons were made by analysis of variance (ANOVA). Scheffé test was used for post hoc evaluation of difference among groups. In all statistical evaluations, $p < 0.05$ was considered as statistically significant.
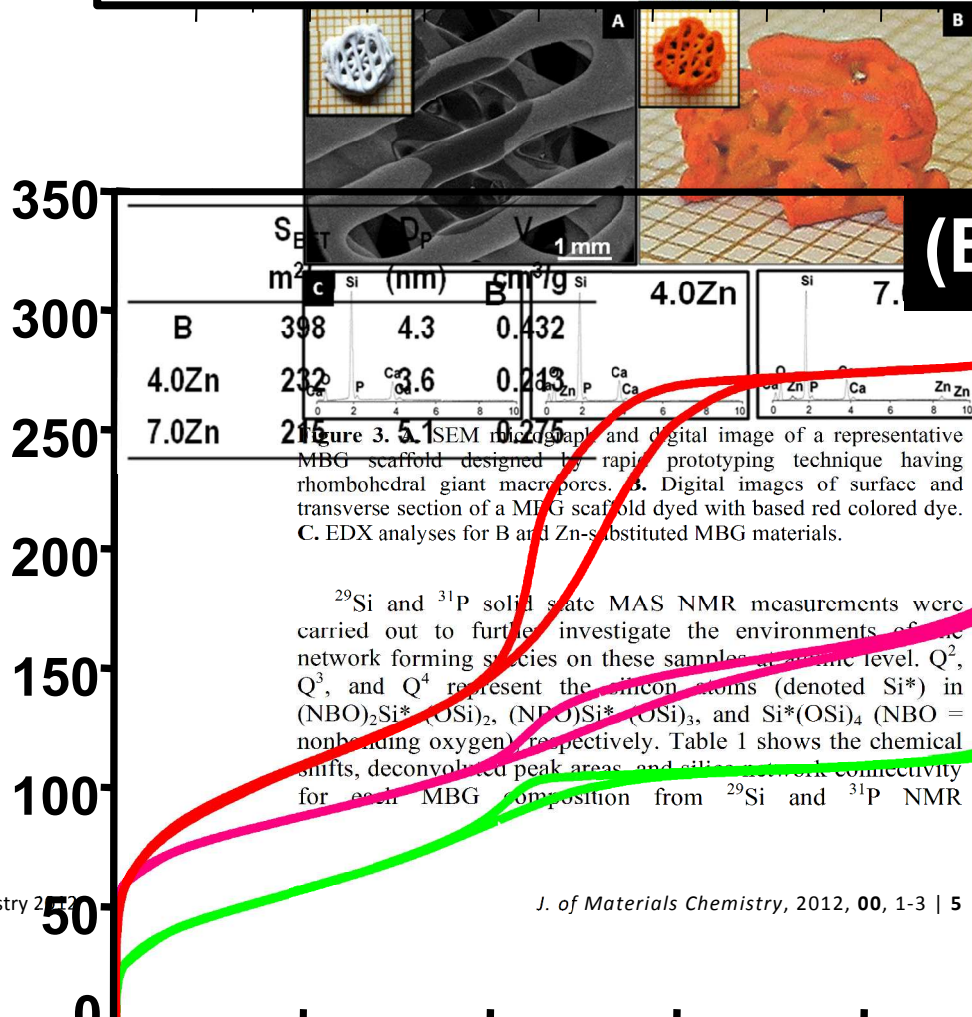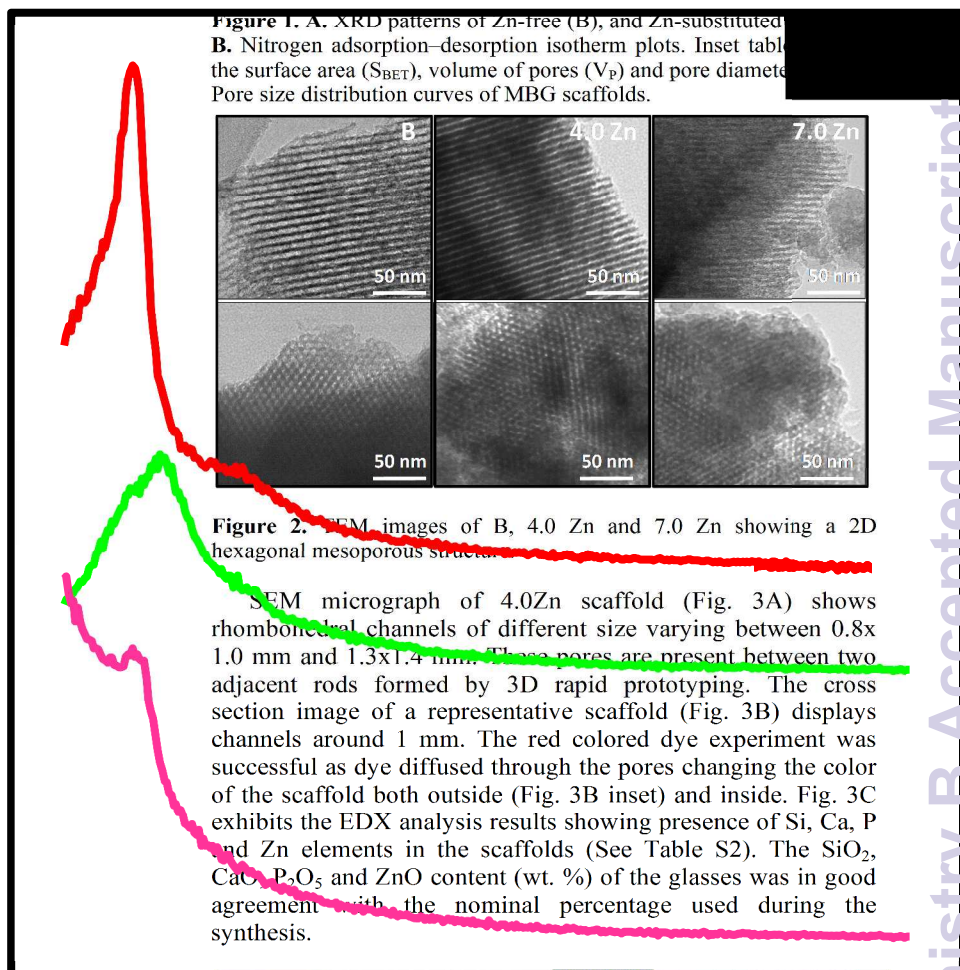
3. Results and discussion

3.1. Characterization of zinc substituted and non-substituted MBG scaffolds

Low-angle XRD analysis was carried out to explore the possible mesopore order in the fabricated scaffolds. Fig. 1A collects the XRD patterns of B, 4.0Zn and 7.0Zn scaffolds after calcination. B showed a sharp diffraction maximum at 2θ in the region of $1.0° - 1.4°$ assigned to (10) reflection, along with a poorly resolved peak at around 2.3° that can be assigned to (11) reflection. These maxima were indexed on the basis of an ordered 2D hexagonal structure (*p6mm* plain group) by assuming TEM results that will be presented later. As it can be observed, the intensity of the XRD maxima decreases with the increase of the ZnO content in the MBGs, indicative of a partial deterioration of the mesoporous order.[28]

Fig. 1B and 1C shows the nitrogen adsorption-desorption isotherms and pore size distributions of B, 4.0Zn and 7.0Zn scaffolds. All curves can be identified as type IV isotherms characteristic of mesoporous materials. The hysteresis loops obtained are type H1 in the mesopore range, which are characteristic of cylindrical pores. All samples show single-model mesopore size distribution centered between 3.6 and 6.3 nm. The pore size distribution relatively wide which is common in this kind of template glasses obtained by EISA method.[10] Table (inset Fig. 1B) compares the textural properties i.e surface area (S_{BET}), determined by using the BET method between the relative pressures (P/P_o) 0.05-0.25, pore diameter (D_P), calculated by the BJH method from the adsorption branch of the isotherm, and total pore volume (V_P), obtained using the t-plot method from the amount of N_2 adsorbed at a P/P_o of 0.97, of MBG scaffolds. Decrease in surface area and pore volume in case of zinc substituted scaffolds were noticed as compared to B scaffold. However, increase in pore size was observed in 7.0Zn scaffolds.[28]

TEM images of B, 4.0Zn and 7.0Zn samples are shown in Fig. 2 taken with the electron beam perpendicular (top) and parallel (down) along to the mesoporous channels, respectively. As it can be observed all the samples exhibit typical 2D-hexagonal ordered mesoporous arrangement. Therefore, the TEM images confirm a loss of order as the ZnO content in the pores increased as it was already showed by XRD.

Figure 1. A. XRD patterns of Zn-free (B), and Zn-substituted
B. Nitrogen adsorption–desorption isotherm plots. Inset table
the surface area (S_{BET}), volume of pores (V_P) and pore diamete
Pore size distribution curves of MBG scaffolds.

Figure 2. TEM images of B, 4.0 Zn and 7.0 Zn showing a 2D
hexagonal mesoporous structure

SEM micrograph of 4.0Zn scaffold (Fig. 3A) shows
rhombohedral channels of different size varying between 0.8x
1.0 mm and 1.3x1.4 nm. These pores are present between two
adjacent rods formed by 3D rapid prototyping. The cross
section image of a representative scaffold (Fig. 3B) displays
channels around 1 mm. The red colored dye experiment was
successful as dye diffused through the pores changing the color
of the scaffold both outside (Fig. 3B inset) and inside. Fig. 3C
exhibits the EDX analysis results showing presence of Si, Ca, P
and Zn elements in the scaffolds (See Table S2). The SiO_2,
CaO, P_2O_5 and ZnO content (wt. %) of the glasses was in good
agreement with the nominal percentage used during the
synthesis.

	S_{BET} m²	D_P (nm)	V_P cm³/g
B	398	4.3	0.432
4.0Zn	232	3.6	0.243
7.0Zn	216	5.1	0.275

Figure 3. A. SEM micrograph and digital image of a representative
MBG scaffold designed by rapid prototyping technique having
rhombohedral giant macropores. **B.** Digital images of surface and
transverse section of a MBG scaffold dyed with based red colored dye.
C. EDX analyses for B and Zn-substituted MBG materials.

^{29}Si and ^{31}P solid state MAS NMR measurements were
carried out to further investigate the environments of the
network forming species on these samples at atomic level. Q^2,
Q^3, and Q^4 represent the silicon atoms (denoted Si*) in
$(NBO)_2Si*(OSi)_2$, $(NBO)Si*(OSi)_3$, and $Si*(OSi)_4$ (NBO =
nonbonding oxygen) respectively. Table 1 shows the chemical
shifts, deconvoluted peak areas, and silica network connectivity
for each MBG composition from ^{29}Si and ^{31}P NMR

spectroscopy. The signals in the region of -110 ppm to -112 ppm come from Q^4, -100 ppm to -103 ppm comes from Q^3. A resonance at approximately -92 ppm comes from Q^2 and in case of 7.0Zn sample at -83 ppm Q^2 is associated to Zn^{2+} ions.[48]

Table 1. Chemical shifts and relative peak areas obtained by Solid-State Single Pulse ^{29}Si and ^{31}P MAS NMR. The areas for the Q^n units were calculated by Gaussian line-shape deconvolutions and their relative populations are expressed as percentages.

| | ^{29}Si | | | | | | | | | ^{31}P | | | |
| | Q^4 | | Q^3 | | Q^2 | | Q^2_{Zn} | | | Q^0 | | Q^1 | |
	CS (ppm)	Area (%)	CS (ppm)	Area (%)	CS (ppm)	Area (%)	CS (ppm)	Area (%)	<Qn>	CS (ppm)	Area (%)	CS (ppm)	Area (%)
B	-111.8	63.2	-102.9	34.3	-92.0	2.5	/	/	3.61	2.0	93.6	-5.2	6.3
4.0%Zn	-112.0	81.5	-103.1	18.5	/	/	/	/	3.81	2.4	96.5	-7.3	3.5
7.0%Zn	-112.4	13.7	-101.9	59.8	-92.0	18.1	-83.3	8.4	2.87	2.2	95.5	-8.6	4.4

^{29}Si NMR spectroscopy was used to evaluate the network connectivity of MBGs as a function of chemical composition <Q^n> (Fig. 4). The MBG sample is characterized by an high percentage of Q^4 and Q^3 species with a network connectivity of 3.61. These data are lower than that found in a previous study (3.75) for isocompositional sol-gel glasses by ^{29}Si single pulse MAS NMR spectra.[31] Probably, the lowering of network connectivity is due to the increment of specific surface area in MBG glasses. In fact, as detected by 1H →31P cross-polarization spectra (2.94), the connectivity of the surface was lower than that found on bulk (data not shown for sake of brevity). The introduction of 4.0% ZnO causes a slightly increase of network connectivity from B samples. When a small amount of ZnO is added Zn acts as a network former with tetrahedral coordination. The ZnO_4 tetrahedra present a negative charge (2-). For this reason, ZnO_4 tetrahedra attract Ca^{2+} ions and calcium acts as network compensator of charge and not as modifier cation. Thus, the number of NBO decreases with an increment of Q^4 species. However, when higher amount of ZnO is added in 7.0Zn sample, the network connectivity drastically decreases (2.87), exhibiting a higher amount of modifier that disrupts the mesophase formation leading to a depolymerized silica network.[31] That is due to the amount of Ca^{2+} ions necessary to act as compensator of charge was higher with respect to that present in the sample composition because part of Ca^{2+} ions are involved in the Q^0 species of P. In this contest, Zn^{2+} ions cannot play the role of network former but they act as network modifier ions causing a depolymerization of silica network.
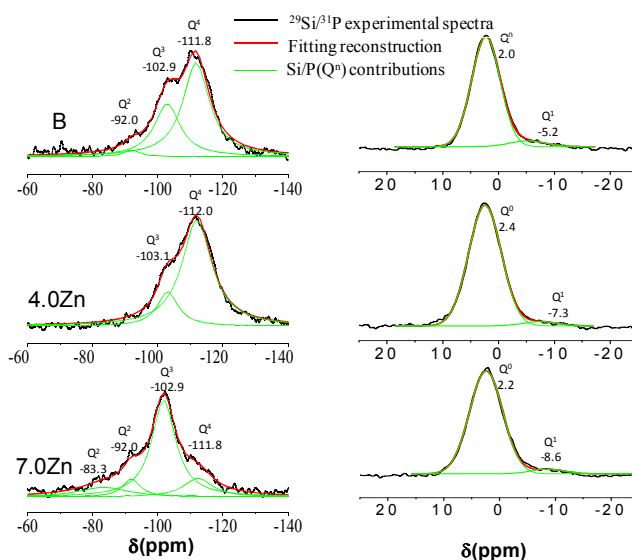
Figure 4. Solid-state ^{29}Si single-pulse (left) and ^{31}P single-pulse (right) MAS/NMR spectra B, 4.0 Zn and 7.0 Zn samples. The areas for the Q^n units were calculated by Gaussian line-shape deconvolutions and are displayed by green (their relative populations are expressed as percentages in Table 1).

Q^0, Q^1, represent phosphorus atoms (denoted P*) present in the PO_4^{3-} species, P*–$(NBO)_4$, $(NBO)_3$-P*–(OP) respectively (NBO denotes a nonbonding oxygen, relative to another P atom). The single-pulse ^{31}P MAS NMR spectra of the materials show a mean maximum of ~2 ppm assigned at the Q^0 environment typical of an amorphous orthophosphate (Fig. 4). A second weak signal sited from -5.2 ppm to -8.6 ppm appears when ZnO % increase in MBGs. This resonance falls in the range of Q^1 tetrahedra and can be assigned to P-O-Si environments as reported in previous studies.[49,50] P is present mainly as orthophosphate units. However, it is interesting to note that the zinc introduction cause a slight decrement of Q^1 units percentage and its chemical shift pass progressively from -5.2 ppm for B to -8.6 ppm for 7.0Zn samples suggesting a partial conversion of P–O–Si units into P–O–Zn units. The formation of P–O–Zn was detected by *Linati L. et al.* in bioactive glasses prepared by fusion where a shift towards lower ppm was detected by the increment of ZnO % in the glass composition.[51]

### 3.2. Biocompatibility of the degradation products of MBG scaffolds

Extracts obtained from B, 4.0Zn and 7.0Zn scaffolds after 2 and 4 days were put in contact with osteoblast-like cells to evaluate the effect of degradation products from scaffolds. In both cases, osteoblast-like cells cultured in the absence of degradation products were used as controls. Fig. 5A shows cell proliferation in the presence of MBGs degradation products where an adequate proliferation rate was observed without any significant difference as compared to control (Fig. 5A). Except in case of B and 7.0Zn scaffolds that show a decrease when compared to control (p<0.05) after 4 days.

No cytotoxic degradation products were released from the samples as no significant difference in the release of U/L LDH was observed with respect to the control, except in case of 4 days degradation products of 7.0Zn scaffolds (p<0.005) (Fig. 5B). These facts indicate that osteoblast in contact with

degradation products from B scaffolds underwent a cytostatic effect. However, we cannot state that the lower proliferation compared to control is due to cytotoxic effect after 4 days.[43]

In Fig. 5C, cells maintained their typical osteoblast morphology in the presence of degradation products from the samples after 2 and 4 days. However 7.0Zn scaffolds leads to some cluster of agglomerate cells that are attached but not spread after 4 days.

The degradation test reveals that no cytotoxic agent was released from scaffolds. Moreover, the cells maintained their morphology for all samples studied, except in case of 7.0Zn scaffolds. LDH assay and cell morphology of this sample clearly indicates that some cytotoxic agent is released from the samples causing cell death. These in vitro results reveal a biocompatible behavior of the degradation products released from B and 4.0Zn scaffolds.
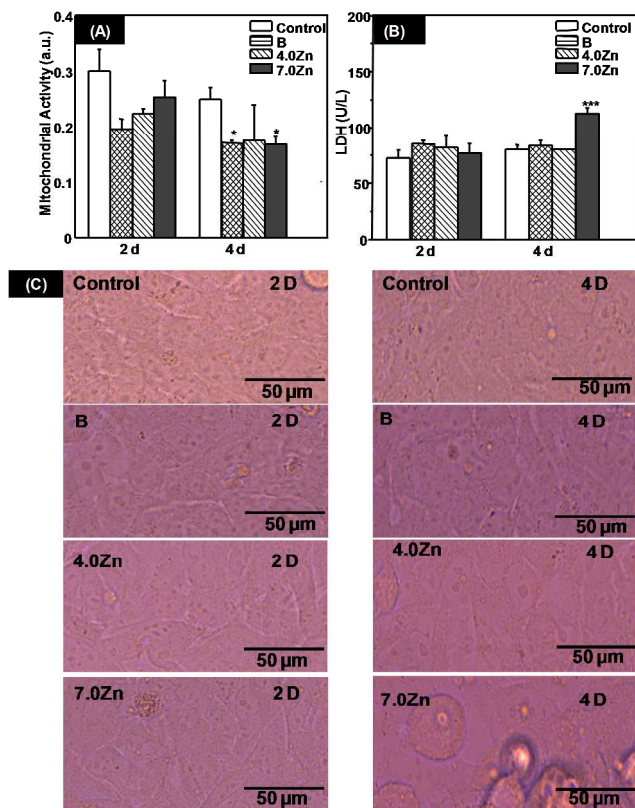

Figure 5. A. MTT proliferation assay of HOS cells in the presence of degradation products released from MBG scaffolds after 2 and 4 days of incubation. **B.** LDH released into the medium from HOS cells cultured in the presence of degradation products after 2 and 4 days. The values shown are means ± standard errors. Significant differences were observed between the control and scaffolds results for both cell proliferation and LDH released *($p<0.05$) and ***($p<0.005$) **C.** Cell morphology evaluation by optical microscopy of HOS cells cultured in the presence of degradation products for 2 and 4 days. The controls correspond to HOS cells incubated in the absence of degradation products.

3.3. Biocompatibility of MBG scaffolds

Fig. 6 shows the osteoblast cells morphology onto B, 4.0Zn and 7.0Zn scaffolds after 2 days of culture. Viable and well-spread cells are observed in close contact with B, 4.0Zn and

7.0Zn scaffold surface. In general, interconnected macropores larger than 100 μm are desirable in scaffolds for bone regeneration. Therefore, the 3D printed MBG scaffolds with channels between 0.8 to 1.4 mm have desirable macroporous structure for bone regeneration in the three samples (Fig. 3). Fig. 6 (bottom right) shows a SEM micrograph of the 4.0Zn scaffold showing the spreading and rather polygonal morphology of osteoblast-like cells attached on the rods of the 3D scaffold (indicated by arrows). Two levels, level 1 (L1) constituting the most external layer of the scaffold and level 2 (L2) denotes rods forming the subsequent internal layer of it.
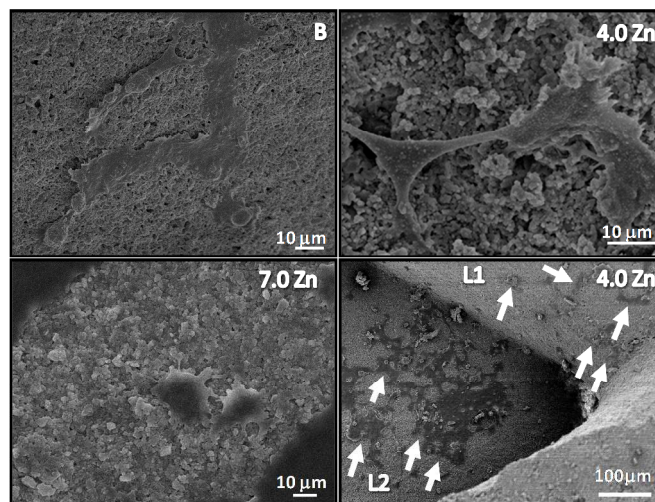
Figure 6. SEM micrographs of 2 days cultured surface of B, 4.0Zn and 7.0Zn MBG scaffolds. SEM micrograph of the 4.0 Zn scaffold surface showing the internalization and colonization of HOS cells after 2 days of culture. The external level (L1) and the internal level (L2) indicate osteoblasts colonization (indicated by arrows).

Cell proliferation was measured in terms of mitochondrial activity on B, 4.0Zn and 7.0Zn scaffolds after 1, 3 and 6 days (Fig. 7A). Tissue culture plastic plate was used as a control. B and 4.0Zn scaffolds show an increase in the levels of proliferation as a function of incubation time on both scaffolds and bottoms of the cell culture wells. Moreover, proliferation on 4.0Zn scaffolds was higher than that of B scaffolds after 6 days. However, 7.0Zn scaffolds only exhibited an adequate proliferation until 3 days.
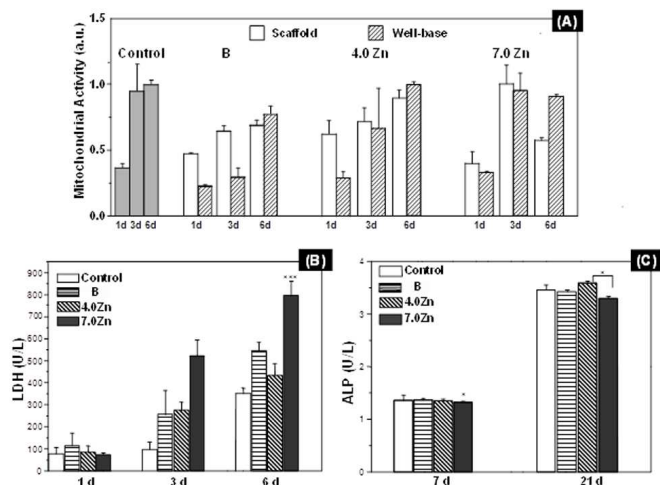
To evaluate the cytotoxic effect of the different materials the amount of LDH release to osteoblast-like cells culture in the presence of the different scaffolds was determined after 1, 3 and 6 days (Fig. 7B). B and 4.0Zn scaffolds indicated that no cytotoxic agent was released, without any significant differences in U/L LDH level with respect to control was observed. However, an increase of LDH level ($p<0.005$) compared to control and low proliferation onto 7.0Zn scaffolds indicate a cytotoxic effect after 6 days.

Fig. 7C shows the ALP activity after 7 and 21 days of incubation of the cells on MBG scaffolds. ALP is an early marker of the osteoblast phenotype and is up regulated at the onset of osteoblast differentiation.[34] The results obtained reveal a positive effect on osteoblast differentiation on cell attached to scaffolds showing no significant differences from the control except onto 7.0 Zn surface (p< 0.05) due to cytotoxic effect after 7 days. As it can be observed that at 21 days the ALP levels are three times higher than at 7 days. After 21 days, 4.0Zn scaffolds exhibit a significantly higher ALP activity than

7.0Zn scaffolds (p<0.05), indicating that 4.0Zn scaffolds present more adequate composition for biocompatible behavior.

Fig. S1 (Supplementary Information), shows the FTIR spectra of all the scaffolds after being soaked up to 7 days in complete medium at 37 ºC. Before soaking, the spectra are similar to bioactive silica glasses exhibiting bands of Si–O at 1050, 802 and 470 cm^{-1}. After soaking, new bands appear in the spectra, mainly in the region of phosphate groups. In general, an easy way to evaluate the in vitro bioactive response of a glass is by measuring the time required to detect the band at 565 cm^{-1}, characteristic of amorphous phosphate, and the doublet at 560 and 600 cm^{-1}, characteristic of

Figure 7. A. MTT proliferation assays of osteoblast cells seeded on well base of culture plate and on B, 4.0Zn and 7.0Zn MBG scaffolds after 1, 3 and 6 days of culture under standard conditions. No significant differences were observed. **B.** LDH released into the medium from osteoblast cells cultured in the presence of MBG scaffolds. **C.** Cellular differentiation assays measuring ALP activity (ALP U/L) of osteoblast cells seeded on B, 4.0Zn and 7.0Zn MBG scaffolds after 7 and 21 days under standard conditions. The values shown are means ± standard errors for all the assays. The control is ostoblast cells in absence of scaffolds. Significantly different in respect to the controls and rest of the series (*p<0.05 and ***p<0.005).

crystalline phosphate.[31] For B scaffolds, the amorphous phosphate was formed after 2 days and the crystalline phosphate at 4 days. However, for 4.0Zn and 7.0Zn only the band of amorphous phosphate was visible after 7 days indicating that the presence of Zn in the glass considerably retarded the in vitro bioactive process.[31]

Indeed, complete medium is not the ideal solution to evaluate the in vitro bioactivity of a glass which is generally performed in Simulated Body Fluid (SBF). However, we carried out this study because complete medium was used for the cell culture studies and it is necessary to know the surface reactivity on the investigated samples. Results included in Fig. S1 confirms quick in vitro bioactive response of mesoporous glasses. For instance, B sample surface was covered by crystalline phosphate after only 4 days of soaking, [52] even in an in vitro solution rich in proteins like the complete medium which hinder the amorphous phosphate crystallization.

To better understand the samples cytocompatibility, the variation of calcium, phosphorous, silicon and zinc ionic concentration in solution was also measured (see Fig. 8). In B the calcium concentration underwent an initial increase followed by a sudden decrease reaching a value of 10 ppm after 2 days of study. This variation agrees well with the amorphous

phosphate formation at this time detected by FTIR spectroscopy. That would indicate a lower level of proliferation and a cytostatic effect on its degradation products compared to 4.0Zn scaffolds. However, in 4.0Zn and 7.0Zn scaffolds the calcium decrease was slower and its concentration was still higher than in B scaffolds after 7 days. After 6 days, the increase in the calcium concentration was high in all the samples but far below the toxicity level.[38]
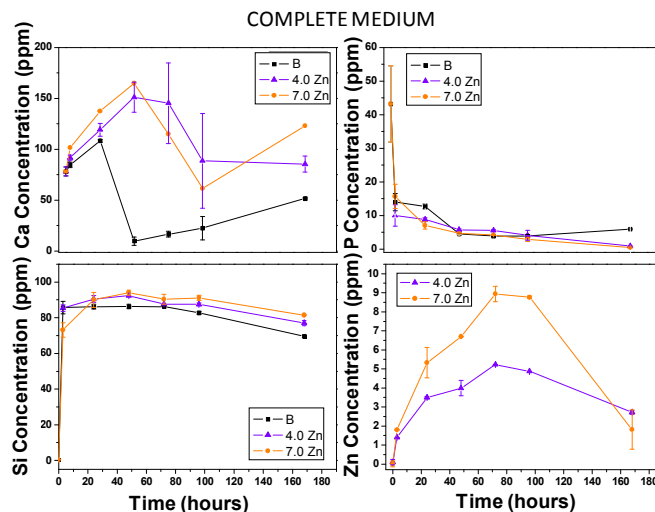

Figure 8. Evolution of calcium, phosphorous, silicon and zinc content in complete medium as a function of time when non seeded MBG scaffolds are soaked

On the other hand, the variation of the concentration profile of P drastically decreased in the first 3 h followed by release-precipitation equilibrium. Indeed after 2 days, P level in solution practically disappeared for the three samples. This can be attributed to the apatite layer formation in B, and to the calcium and zinc phosphate mix deposition for 4.0Zn and 7.0Zn scaffolds.[29] On the other hand, in the three samples Si concentration increased up to 80-90 ppm in first 72 h, which agrees well with the values of 60-70 ppm reached in pure water at 25°C in the pH 5-8 range for silica materials.[53] However, the later decreasing trend could be probably due to the formation of a silica gel rich layer on the glass surface.[54]

A different trend was found in the zinc evolution in Zn-substituted scaffolds. The Zn concentration increased during 72 h in both 4.0Zn and 7.0Zn samples. Reaching a value of 9 ppm in 7.0Zn scaffolds, that was double the amount found in 4.0Zn (4.7 ppm) scaffolds. The higher dissolution when amount of zinc increase, agree with the silica network depolymerization observed in NMR for 7.0Zn samples where more Zn^{2+} ions occupy positions of network modifiers and consequently are easily released to the medium. After 4 d, both samples showed a decrease in Zn level reaching values close to 2–3 ppm. This decrease could be due to zinc phosphate formation explained in our previous study.[28]

Therefore, the biocompatibility of MBG scaffolds is greatly influenced by their composition.[55,56] Ionic dissolution products released from the scaffolds have intense effect on osteoblast cell development.[57] In the present work, it can be observed the effect of incremental amount of zinc on MBG glass scaffolds plays a different behavior onto osteoblast-like cells. Osteoblasts cells exhibited excellent adhesion onto scaffolds surface, increased proliferation and differentiation without cytotoxic

effect, when the amount of zinc on MBG glass scaffolds was 4.0% ZnO (Figs. 6 and 7). This biocompatible behavior is related with the higher silica network connectivity of 4.0Zn structure compared with 7.0Zn detected by NMR (Table 1). However, the presence of higher amount of zinc in MBG scaffolds (7.0% ZnO) implies less cell development and cytotoxic effect comparing to B and 4.0Zn samples at long period of time. The incorporation of zinc (4.0% and 7.0%) into MBG scaffolds show controlled release of Zn^{2+} with maximum value reaching up to 5 ppm and 9 ppm, respectively. Previous studies have shown that the incorporation of 5% ZnO in bioactive glasses of other glass systems is the maximum amount that exhibit a no cytotoxic effect and enhance the osteoblast cell development.[26,58–60] Yamamoto et al. demonstrated that a zinc release of 5.89 ppm inhibits normal osteoblast function.[61] This behavior was found in case of 7.0Zn scaffolds that showed zinc release up to 9 ppm after 3 days. Hence, it resulted into cell death observed from the high LDH value (Fig. 7B). This was further confirmed by in vitro biocompatibility of the degradation products that also showed high cytotoxic levels after 4 days of incubation in complete medium (Fig. 5B). Higher amount of zinc released to the medium is due to silica network depolymerization, observed in NMR results. The cross-linking degree, directly related to the amount of silanol groups on the matrix surface, could affect the cells development. Several authors[62,63] have demonstrated that both distribution and abundance of surface silanol groups determine the cytotoxicity degree of a nanostructured material. In the present study, 7.0Zn scaffolds exhibit 1.3 fold higher silica network depolymerization than B and 4.0Zn scaffolds, which could be enough to provoke a cytotoxic effect on osteoblast cells of 7.0Zn composition.

### 3.4. Antibacterial properties of MBG scaffolds

Fluorescence based Live/Dead Baclight bacterial viability test provides useful information about the membrane integrity of *S. aureus*, indicating the bacteria viability after 2 days in THB at 37ºC (Fig. 9A). During the study of *S. aureus*, analysis of B scaffolds clearly showed zones with minimal red fluorescence reflecting the presence of large percentage (~ 75%) of viable cells (Fig. 9B). In case of zinc substituted MBG scaffolds, this percentage dropped to 30 and 10% with 4.0Zn and 7.0Zn MBG scaffolds respectively, showing noticeable loss in viable bacteria. The results clearly indicate that presence of zinc hinders *S. aureus* biofilm formation and the impact increases with increase in percentage of zinc in the structure of meso-macroporous scaffolds (p <0.005).

Fig. 10 shows variation in ion concentration of THB medium in which B, 4.0Zn and 7.0Zn MBG scaffolds were soaked without bacteria between 3 hours and 7 days. The main difference in inorganic ion concentration between THB and complete medium was initial calcium in media. In fact, in THB it was zero while in complete medium was around 75 ppm. However, the concentration of P in THB and complete medium was similar, 40 and 55 ppm, respectively.

In B and 4.0Zn level of calcium increased up to 2 days and then later decreased. While in 7.0Zn sample the increment of calcium level can be seen up to 3 days and then show sudden fall in concentration. The maximum value of calcium concentration was inversely proportional to zinc content. In fact the concentrations were 188, 390 and 420 ppm for B, 4.0Zn and 7.0Zn samples, respectively. These values could appear surprisingly higher than that found in complete medium.

Moreover, if we assume all P was used in the HA formation, the solubility limit for the next available calcium compound after all calcium phosphates have formed would be $CaCO_3$. $CaCO_3$ has a solubility limit of around 70 ppm in water in presence of CO_2. However, in the THB solution 20g/L of Yeast enriched peptone is present. It is well known that Ca ions has the ability to form a complex with peptones.[64] In fact in a solution containing 0.01M (400 ppm) of calcium ions at pH=7 around 80% of calcium ions are complexed with peptone. Thus, this explained the calcium level found in THB medium.

P and Si concentration trend for all samples was similar. P level show sudden decrease and then remain constant around ~ 10 ppm. On the other hand, Si concentration increased in first 2 days but later remain constant around ~ 30 - 40 ppm. Moreover, P and Si behavior was similar to complete medium.
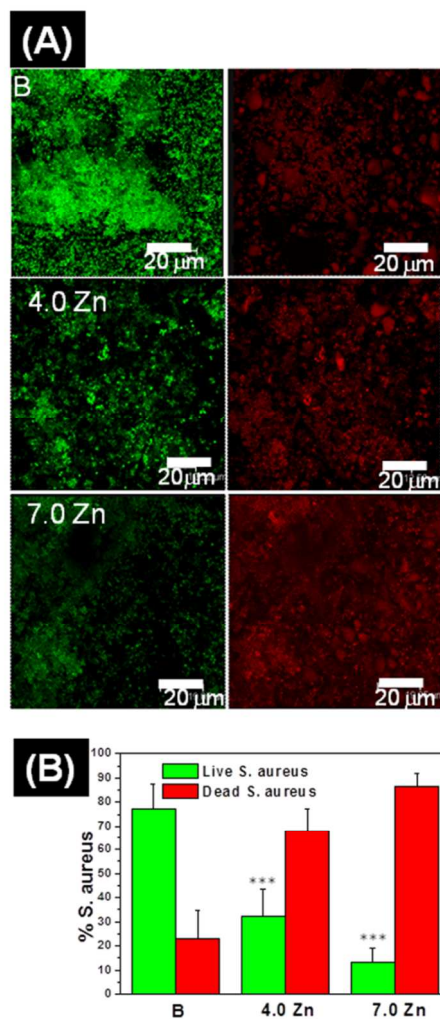
Figure 9.A. Representative confocal micrographs of *S. aureus* biofilms formed onto MBG scaffold surfaces after 2 days soaked in THB. Viable (green) and non-viable (red) bacteria are shown. **B.** The percentage of surface area covered with dead and live bacteria was calculated using ImageJ software. The assays values shown are means ± standard errors. ***Significantly different in respect to B scaffolds (*p<0.005*).

Zinc substituted MBG scaffolds both 4.0Zn and 7.0Zn showed similar zinc evolution than in complete medium. Level of Zn on 4.0% Zn and 7.0% Zn scaffolds first increased to

almost 4.8 and 7.0 ppm after 3 days, respectively. After that, a decrease in Zn level reaching up to 2 – 3 ppm for both samples.

Further, the FTIR analysis of B, 4.0Zn and 7.0Zn MBG scaffolds soaked in THB was done to confirm apatite layer formation (Fig. S2, Supporting Information). The behavior of samples was similar to that observed when they were soaked in complete medium. The analysis confirms the apatite layer formation in B sample after 2 days. However, for 4.0Zn and 7.0Zn scaffolds, amorphous calcium/zinc phosphate formation was observed instead of apatite layer which is due to lower solubility product constant of $Zn_3(PO_4)_2$ than $Ca_3(PO_4)_2$. So in aqueous solution PO_4^{3-} ion prefers to combine with Zn^{2+} ions rather than calcium.[65]

agents.[67] The results demonstrate that zinc containing MBG scaffolds kills the majority of bacteria after biofilm formation and dead bacteria are significantly higher when increase the amount of zinc on MBGs.

Bioactive sol-gel glass must exhibit an adequate antibacterial activity and show a biocompatible behavior with no cytotoxic effect. Thus, it would lead to a decrease in the infection rates after implantation surgery at the same time of a new bone formation in the surgery zone. Thus, the present study demonstrates that 4.0Zn scaffolds could be a potential candidate for bone tissue regeneration due to its biocompatibility and therapeutic potential in treating bone diseases.

Conclusions

This manuscript reports for the first time the synthesis and design by rapid prototyping technique meso-macroporous 3D scaffolds of Zn substituted MBGs with antibacterial properties and a good biocompatible behaviour. B and 4.0Zn MBGs scaffolds showed a good biocompatibility behavior in terms of adhesion, proliferation, differentiation and no cytotoxic degradation products. Moreover, 4.0Zn and 7.0Zn scaffolds, under in vitro conditions simulating severe infection, exhibited 2.8 and 3.6 fold higher *S. aureus* inhibition capacity than non-zinc substituted MBG scaffolds. Thus, the composition and 3D-architecture design of MBGs allows a controlled zinc release which greatly influences the osteoblast cell development. Furthermore, the ions release provides bacteria growth inhibition capacity that would lead to a decrease in the infection rates after implantation surgery. The multifunctional characteristics of studied MBGs scaffolds are suggested to be of great potential to regenerate lost bone tissue.
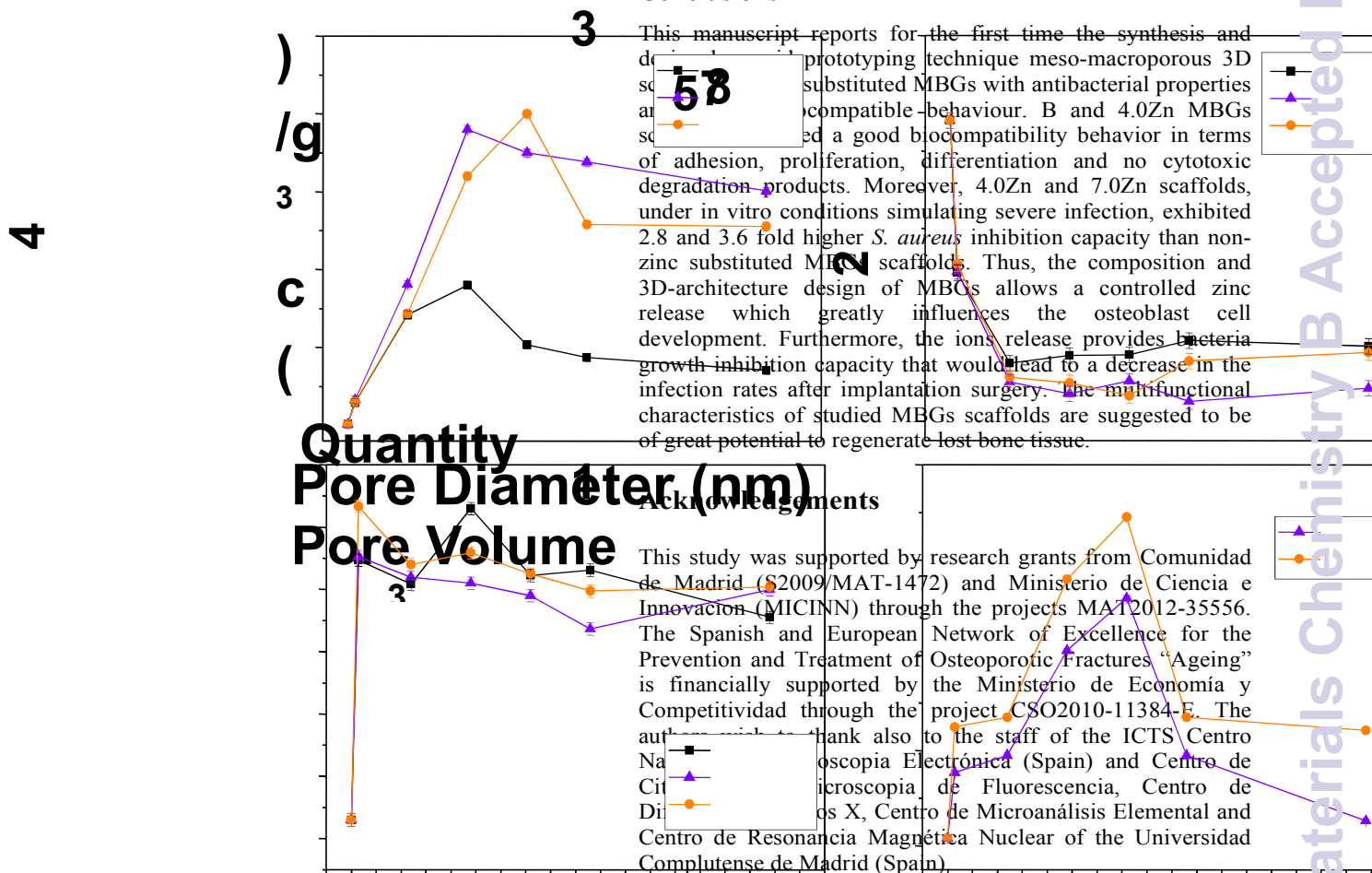
Figure 10. Evolution with time of the calcium, phosphorous, silicon and zinc concentrations in THB medium when non seeded bacteria on MBG scaffolds are soaked.

As it was explained, following the idea of incorporating bioinorganic elements in the bioceramic used in dentistry or orthopedics it is possible to fight the infection on its own. Zinc inhibits multiple activities in the bacterial cell, such as glycolysis, transmembrane proton translocation and acid tolerance.[66] It has been shown to exhibit an antibacterial effect at considerably lower concentrations than many antimicrobial

Notes and references

[a] Departamento de Química Inorgánica y Bioinorgánica. Facultad de Farmacia. Universidad Complutense de Madrid. Plaza Ramón y Cajal s/n. 28040 Madrid. Spain.

[b] Networking Research Center on Bioengineering, Biomaterials and Nanomedicine (CIBER-BBN), Madrid, Spain.

[c] I+12 Instituto Investigación 12 de Octubre Madrid, Spain

[d] Department of Chemical and Geological Sciences, University of Modena and Reggio Emilia, Via G. Campi 183, 41125 Modena, Italy

[*] Corresponding author: E-mail address, vallet@ucm.es, salinas@ucm.es

1 W. Zimmerli, A. Trampuz and P. E. Ochsner. *N. Engl. J. Med.,* 2004, **351**, 1645-54.

2 J. L. Del Pozo and R. Patel. *N. Engl. J. Med.,* 2009 **361**, 787–794.

3 M. Ribeiro F. J. Monteiro and M. P. Ferraz, *Biomatter.*, 2012 **2:4**, 176-194.

4 C. M. Brandt, W. W. Sistrunk, M. C. Duffy, A. D. Hanssen, J. M. Steckelberg, D. M. Ilstrup and D. R. Osmon, *Clin. Infect. Dis.,* 1997, **4**, 914-9.

5 M. Kazemzadeh-Narbat, J. Kindrachuk, K. Duan, H. Jenssen, R. E. W. Hancock and R. Wang. *Biomaterials* 2010, **31**, 9519–26.

6 A. Simchi, E. Tamjid, F. Pishbin and A. R. Boccaccini. Nanomed. Nanotechnol. Biol. Med., 2011, **7**, 22–39.

7 J. Esteban and J. Cordero-Ampuero. *Expert Opin. Pharmacother.,* 2011; **12**, 899–912.

8 R. M. Donlan. *Emerg. Infect. Dis.,* 2002, **8**, 881-890.

9 X. Yan, C. Yu, X. Zhou, J. Tang and D. Zhao. *Angew. Chem. Int. Ed.,* 2004, **43**, 5980 –4.

10 A. Lopez-Noriega, D. Arcos, I. Izquierdo-Barba, Y. Sakamoto, O. Terasaki and M. Vallet-Regi. *Chem. Mater.,* 2006, **18**, 3137–44.

11 I. Izquierdo-Barba and M. Vallet-Regí. *Solid State Sci.,* 2011, **13**, 773–83.

12 C. Wu and J. Chang. *Interface Focus,* 2012, **2**, 292–306.

13 I. Izquierdo-Barba, A. J. Salinas and M. Vallet-Regí. *Int. J. Appl. Glass Sci.*, 2013, **4**, 149–61.

14 W. Xia and J. Chang. *J. Control. Release,* 2006, **110**, 522–30.

15 D. Arcos and M. Vallet-Regí. *Acta Biomater.,* 2010, **6**, 2874–88.

16 M. Zhu, L. Zhang, Q. He, J. Zhao, G. Limin and J. Shi, *J. Mater. Chem.*, 2011, **21**, 1064–72.

17 Y. Zhu, C. Wu, Y. Ramaswamy, E. Kockrick, P. Simon, S. Kaskel and H. Zreiqat. *Micropor. Mesopor. Mater.,* 2008, **112**:, 494–503.

18 X. Wang, X. Li, A. Ito and Y. Sogo. *Acta Biomater.*, 2011; **7**, 3638–44.

19 D. W. Hutmacher. *Biomaterials,* 2000, **21**, 2529–43.

20 C. Wu, Y. Luo, G. Cuniberti, Y. Xiao and M Gelinsky. *Acta Biomater.*, 2011, **7**, 2644–50.

21 A. J. Salinas and M Vallet-Regi. *RSC Adv.*, 2013, **3**, 11116 –31.

22 C. Wu, Y. Zhou, M. Xu, P. Han, L. Chen, J. Chang and Y. Xiao. *Biomaterials*. 2013, **34**, 422–33.

23 J. Isaac, J. Nohra, J. Lao, E. Jallot, J. Nedelec, A. Berdal and J. M. Sautier. Eur. Cells. Mater., 2011, **21**, 130–43.

24 C. Wu, Y. Zhou, W. Fan, P. Han, J. Chang, J. Yuen, M. Zhang and Y. Xiao. *Biomaterials*, 2012, **33**, 2076–85.

25 D. Boyd, G. Carroll, M. R. Towler, C. Freeman, P. Farthing and I. M. Brook. *J. Mater. Sci: Mater. Med.*, 2009, **20**, 413–20.

26 G. Lusvardi, G. Malavasi, L. Menabue, M. C. Menziani, A. Pedone, U. Segre, V. Aina, A. Perardi, C. Morterra, F. Boccafoschi, S. Gatti, M. Bosetti and M. Cannas. *J. Biomater. Appl.,* 2008, **22**, 505–26.

27 X. Li, X. Wang, D. He and J. Shi. *J. Mater. Chem.,* 2008, **18**, 4103–4109.

28 A. J. Salinas, S. Shruti, G. Malavasi, L. Menabue and M. Vallet-Regí. *Acta Biomater.*, 2011, **7**, 3452–8.

29 S. Shruti, A. J. Salinas, G. Lusvardi, G. Malavasi, L. Menabue and M. Vallet-Regi. *Acta Biomater.,* 2013, **9**, 4836–44.

30 S. Shruti, A. J. Salinas, E. Ferrari, G. Malavasi, G. Lusvardi, A. L. Doadrio, L. Menabue and M. Vallet-Regi. *Micropor. Mesopor. Mater.,* 2013, **180**, 92–101.

31 S. Shruti, A. J. Salinas, G. Malavasi, G. Lusvardi, L. Menabue, G. Ferrara P. Mustarelli and M. Vallet-Reg. *J. Mater. Chem.,* 2012, **22**, 13698–706.

32 S. L. Hall, H. P. Dimai and J. R. Farley. *Calcif. Tissue Int.,* 1999, **64**, 163–72.

33 L. Fong, K. Tan, C. Tran, J. Cool, M. Scherer, R. Elovaris, P. Coyle, B. K. Foster, A. M. Rofe and CJ Xian. *Bone* 2009, **44**, 1151–62.

34 A. Hoppe, S. G. Nusret and A. R. Boccaccini. *Biomaterials,* 2011, **32**, 2757–74.

35 A. Ito, H. Kawamura, M. Otsuka, M. Ikeuchi, H. Ohgushi, K. Ishikawa K. Onuma, N. Kanzaki, Y. Sogo and N. Ichinose. *Mater. Sci. Eng. C,* 2002, **22**, 21–5.

36 Y-H. Cho, S-J. Lee, J. Y. Lee, S. W. Kim, C. B. Lee, W. Y. Lee and M. S. Yoon. *Int. J. Antimicrob. Agents,* 2002, **19**, 576-582.

37 A. B. Lansdown, U. Mirastschjiski, N. Stubbs, E. Scanlon and M. S. Agren. *Wound Repair Regen.,* 2007, **15**, 2–16.

38 A. Hoppe, V. Mouriño and A. R. Boccaccini. *Biomater. Sci.,* 2013, **1**, 254–6.

39 I. Nikolic-Hughes, P. J. O'Brien and D. Herschlag. *J. Am. Chem. Soc.,* 2005, **127**, 9314–5.

40 V. Aina, A. Perardi, L. Bergandi, G. Malavasi, L. Menabue, C. Morterra and Ghigo D. *Chemico-Biological Interactions,* 2007, **167**: 207–18.

41 S. Brunauer, P. H. Emmet and E. Teller. *J. Am. Chem. Soc.*, 1938, **60**, 309–19.

42 E. P. Barrett, L. G. Joyner and P. P. Halenda. *J. Am. Chem. Soc.,* 1951, **73**, 373–80.

43 S. Sánchez-Salcedo, I. Izquierdo-Barba, D. Arcos and M. Vallet-Regí. *Tissue Eng.*, 2006, **12**, 279–90.

44 N. Olmo, J. Turnay, G. González de Buitrago, I. López de Silanes, J. G. Gavilanes and M. A. Lizarbe. *Eur. J. Biochem.,* 2001, **268**, 2113–23.

45 S. Sánchez-Salcedo, M. Colilla, I. Izquierdo-Barba and M. Vallet-Regí. *J. Mater. Chem. B*, 2013, **1**, 1595–606.

46 A. H. Redd and C. B. Huggins. *Proc. Soc. Exp. Biol. Med.*, 1972, **140**, 807–10.

47 L. Boulos, M. Prevost, B. Barbeau, J. Coallier and R. Desjardins. *J. Microbiol. Methods*, 1999, **37**, 77–86.

48 M. Goswami, G. P. Kothiyal, L. Montagne and L. Delevoye. *J. Solid State Chem.,* 2008, **181**, 269–75.

49 E. Leonova, I. Izquierdo-Barba, D. Arcos, A. Lopez-Noriega, N. Hedin, M. Vallet-Regì and M. Eden. *J. Phys. Chem. C,* 2008, **112**, 5552–62.

50 A. Garcıa, M. Cicuendez, I. Izquierdo-Barba, D. Arcos, and M. Vallet-Regí. *Chem. Mater.*, 2009, **21**, 5474–84.

51 L. Linati, G. Lusvardi, G. Malavasi, L. Menabue, M. C. Menziani, P. Mustarell and U. Segre. J. Phys. Chem. B, 2005, **109**, 4989–98.

52 A. J. Salinas and M. Vallet-Regí, in *Surface Tailoring of Inorganic Materials for Biomedical Applications*. L. Raimondi, C. Bianchi and E. Verné (eds), Bentham Science Publishers, 359–37, 2012.

53 G. B. Alexander, W. M. Heston and R. K. Iler. *J. Phys. Chem.,* 1954, **58**, 453–5.

54 L. L. Hench. *J. Am. Ceram. Soc.,* 1991, **74** , 1487—510.

55 P. Valerio, M. M. Pereira, A. M. Goes and M. F. Leite. *Biomaterials*, 2004, **25**, 2941–8.

56 A. El-Ghannam, P. Ducheyne and I. M. Shapiro. *Biomaterials*, 1997, **18**, 295–303.

57 M. N. Rahaman, D. E. Day, B. S. Bal, Q. Fu, S. B. Jung, L. F. Bonewald and A.P. Tomsia. *Acta Biomater.*, 2011, **7**, 2355–73.

58 S. Haimi, G. Gorianc, L. Moimas, B. Lindroos, H. Huhtala, S. Räty, H. Kuokkanen, G. K. Sandor, C. Schmid, S. Miettinen and R. Suuronen. *Acta Biomater.,* 2009, **5**, 3122–31.

59 V. Salih, A. Patel and J. C. Knowles. Biomed Mater., 2007, **2**, 11–20.

60 V. Aina, G. Malavasi, P. A. Fiorio, L. Munaron and C. Morterra. *Acta Biomater.*, 2009, **5**, 1211–22.

61 A. Yamamoto, R. Honma and M. Sumita. J. Biomed. Mater. Res., 1998, **39**, 331–40.

62 S. Lee, H.S. Yun, S.H. Kim. *Biomaterials.,* 2011, 32, 9434–9443.

63 M. Cicuéndez, I. Izquierdo, M.T. Portolés, M. Vallet-Regí. Eur. *J. Pharm. Biopharm.* 2013, 84, 115-124.

64 L. J. Greenfield. *Ann. NY Acad. Sci.,* 1963, **109**, 23-45.

65 L. R. Du and J. Chang. *J. Bio-Med. Mater. Eng.,* 2006, **16**, 229–36.

66 T. N. Phan, T. Buckner, J. Sheng, J. D. Baldeck and R. E. Marquis. *Oral Microbiol. Immunol.*, 2004, **19**, 31–8.

67 M. G. Brading, V. J. Cromwell, N. M. Jones, J. D. Baldeck and R. E. Marquis. Int. Dent. J., 2003, **53**, 363–70.

GRAPHICAL ABSTRACT

The biocompatibility and the antibacterial capability of meso-macroporous bioactive glass scaffolds in the SiO_2–CaO–P_2O_5–ZnO system were investigated. Zn^{2+} ions release greatly influenced the osteoblast cells development and provides antibacterial capability against S. aureus bacteria.